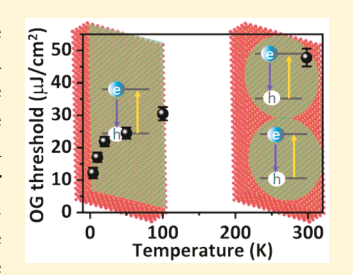


Reducing the Optical Gain Threshold in Two-Dimensional CdSe Nanoplatelets by the Giant Oscillator Strength Transition Effect

Qiuyang Li,[†] Qiliang Liu,[†] Richard D. Schaller,^{‡,§} and Tianquan Lian*,[†]

Supporting Information

ABSTRACT: Two-dimensional CdSe nanoplatelets are promising lasing materials. Their large lateral areas reduce the optical gain threshold by increasing the oscillator strength and multiexciton lifetimes but also increase the gain threshold by requiring multiple band-edge excitons (>2) to reach the optical gain. We observe that the optical gain threshold of CdSe nanoplatelets at 4 K is ~4-fold lower than that at room temperature. Transient absorption spectroscopy measurements indicate that the exciton center-of-mass coherent area is smaller than the lateral size at room temperature and extends to nearly the whole nanoplatelets at 4 K. This suggests that the reduction in the optical gain threshold at a low temperature can be attributed to exciton coherent area extension that reduces the saturation number of band-edge excitons to enable biexciton gain and increases the radiative decay rate, consistent with the giant



oscillator strength transition effect. This work demonstrates a new direction for lowering the optical gain threshold of nanomaterials.

ompared to conventional bulk semiconductor lasers, advantages induced by the quantum confinement along all three dimensions, including the tunable lasing wavelength achieved through size-dependent quantum confinement effects. Moreover, the density of states of QDs near the band edge reduces to a Dirac delta function-like distribution so that carriers are concentrated to fewer states, which reduces the optical gain (OG) threshold as fewer injected carriers are required for population inversion.^{2,3} QD lasers have shown promise in recent years, and continuous-wave lasing⁴ and direct current electrical pumped optical gain⁵ in QD films have been reported. Cadmium chalcogenide (CdX, where X = Se, S, or Te) nanoplatelets (NPLs), with atomic-precise thickness (of ~1.2-1.8 nm) and a large lateral dimension (hundreds of square nanometers), make up an emerging class of nanocrystals⁶ and, by some metrics, have shown potential for lasing applications even greater than that of QDs.7-10 The continuous-wave lasing of CdSe NPLs has been reported, and the best reported threshold of amplified spontaneous emission (ASE) of CdSe NPLs is as low as $6 \mu J/cm^2$, which is >1 order of magnitude lower than that in similar QDs^{1,11} and nanorods (NRs). 12 The low optical gain (OG) threshold of NPLs is attributed to low multiple exciton Auger recombination rates, 13-15 large absorption cross sections, 16 and narrow emission peaks (due to precise confinement energy)¹⁷ of these materials, all of which are a consequence of their unique twodimensional (2D) morphology. Compared to QDs, 2D NPLs have much a larger absorption cross section per unit volume, 16 and biexciton Auger lifetimes in NPLs have been shown to increase with their lateral dimension, 13 which would suggest

that increasing lateral size as a potential approach for further reducing the OG threshold. However, the extended lateral dimension of NPLs allows spatially separated excitons, which increases the maximum number of band-edge exciton states (N_S) to >2. Previous studies have shown that in cadmium chalcogenide QDs¹¹ and NPLs, ^{18–20} optical gain is achieved when the band-edge exciton states are just more than halfoccupied. Thus, the OG threshold corresponds to an average number of excitons per nanocrystal (m_{th}) of >1 for QDs and $>N_S/2$ for NPLs (Scheme 1a). As a result, the OG in NPLs is achieved at higher-order (>2) multiexciton states. These higher multiexciton states are generated by the absorption of multiple photons (>2) and are much shorter-lived compared to the biexciton state, both of which increase the OG threshold intensity.

In this paper, we demonstate a new strategy for reducing the OG threshold in NPLs by exploiting the giant oscillator strength transition (GOST) effect in these 2D colloidal quantum well materials. 6,21,22 Because of the atomically precise thickness of 2D CdSe NPLs, the confinement energy is the same along the lateral dimension. It has been suggested that, in the absence of scattering by phonons and surface imperfections, the band-edge transition oscillator strength concentrates to a single transition state with the lowest energy in k-space, giving rise to the GOST effect, and correspondingly, the exciton center-of-mass (COM) delocalization in real space can coherently extend over the entire NPL. ^{6,21,22} This notion is

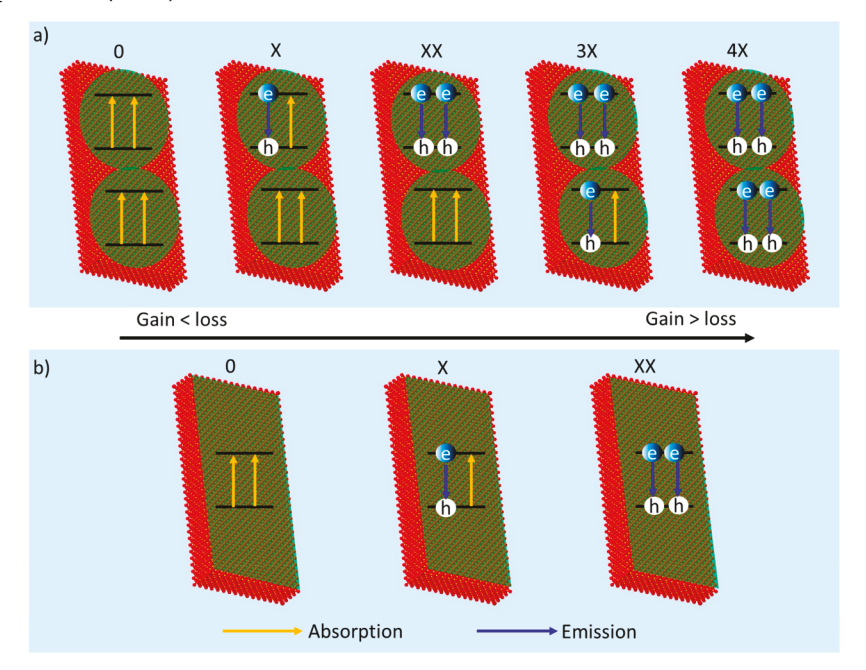
Received: March 16, 2019 Accepted: March 20, 2019 Published: March 20, 2019

Department of Chemistry, Emory University, 1515 Dickey Drive Northeast, Atlanta, Georgia 30322, United States

[‡]Center for Nanoscale Materials, Argonne National Laboratory, Argonne, Illinois 60439, United States

Department of Chemistry, Northwestern University, Evanston, Illinois 60208, United States

Scheme 1. Temperature-Dependent Optical Gain Mechanism, Including (a) a Scheme of Different Exciton States in NPLs at Room Temperature with a Saturation Number of Band-Edge Excitons (N_S) of 4 and (b) a Scheme of Different Exciton States in NPLs at Low Temperatures $(<4 \text{ K})^a$



^aThe exciton center-of-mass coherence was delocalized throughout the whole NPL due to the GOST effect, giving $N_{\rm S}=2$.

supported by the observation of increased radiative decay rate at lower temperatures. 6,21 Note that this COM spatial coherence is different from the temporal coherence of excitonic states, which have been shown to be short-lived (<1 ps). $^{23-25}$ The extent of COM coherent delocalization is often characterized by a coherent spatial area (S_X). We hypothesize that at low temperatures, the COM coherent spatial area can extend to the whole NPL, which results in a doubly degenerate band-edge exciton state (Scheme 1b), similar to QDs, and a greatly enhanced exciton radiative decay rate (GOST effect). The combination of these factors without reducing the large absorption cross section of 2D NPLs should further reduce the OG threshold in 2D NPLs.

Herein, we report a study of the temperature-dependent OG threshold and exciton COM coherent delocalization in colloidal CdSe NPLs using pump fluence-dependent transient absorption (TA) spectroscopy. We observe an ~4-fold lower OG threshold at 4 K compared to that at room temperature (298 K). We develop a new method for direct measurement of $S_{\rm X}$ in colloidal NPLs based on the TA spectroscopic study of the saturation number of band-edge excitons. We show that $S_{\rm X}$ is smaller than the CdSe NPL lateral area at room temperature but increases at lower temperatures until it extends to nearly the NPL lateral area at 4 K. Our results demonstrate the strategy of reducing the OG threshold by the extension of exciton COM spatial coherence and the resulting GOST effect in colloidal NPLs.

For OG studies, we synthesized CdSe NPLs with a thickness of four monolayers (MLs) $(\sim 1.2 \text{ nm})^{2.6}$ following reported procedures with slight modifications. These CdSe NPLs have a zinc-blend structure with four Se layers and five Cd layers and are labeled as NPL1. The transmission electron microscopy (TEM) image of NPL1 (Figure 1a) shows its rectangular shape, from which its lateral size is determined to be $167.8 \pm 27.0 \text{ nm}^2$ (Figures S2c-S4c). Measurements at

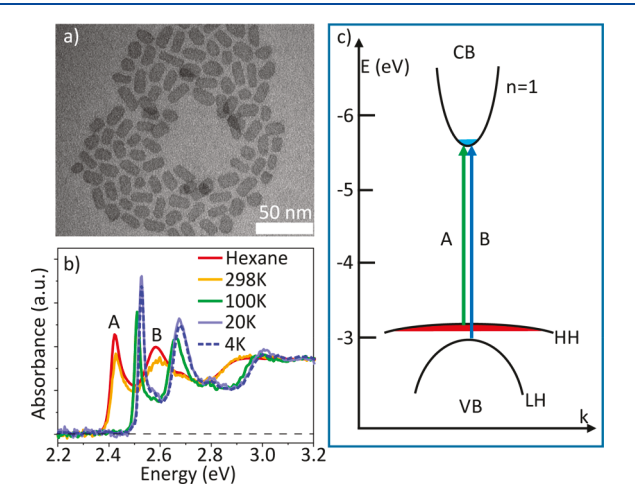


Figure 1. Sample characterization of CdSe NPLs. (a) TEM image of NPL1. (b) Selected absorption spectra of NPL1 in hexane (at 298 K) and PMAO at indicated temperatures. (c) Scheme of the band structure and band-edge transitions of NPL1 at 298 K. HH and LH represent the heavy hole and light hole, respectively. The conduction band (CB) and valence band (VB) positions of NPL1 at room temperature (298 K) are estimated in Supporting Information section S2.

room temperature (298 K) were carried out in solution samples of NPL1 dispersed in hexane. Temperature-dependent measurements (4–298 K) were carried out in thin films of NPL1 dispersed in poly(maleic anhydride-alt-1-octadecene) (PMAO). The sample preparation details are shown in Methods. These polymer-dispersed NPL films instead of solid films of NPLs were used for low-temperature study to reduce the level of stacking of NPLs, which has been reported to cause an additional inter-NPL exciton relaxation pathway, such as Forster energy transfer between NPLs.^{28–30} The

The Journal of Physical Chemistry Letters

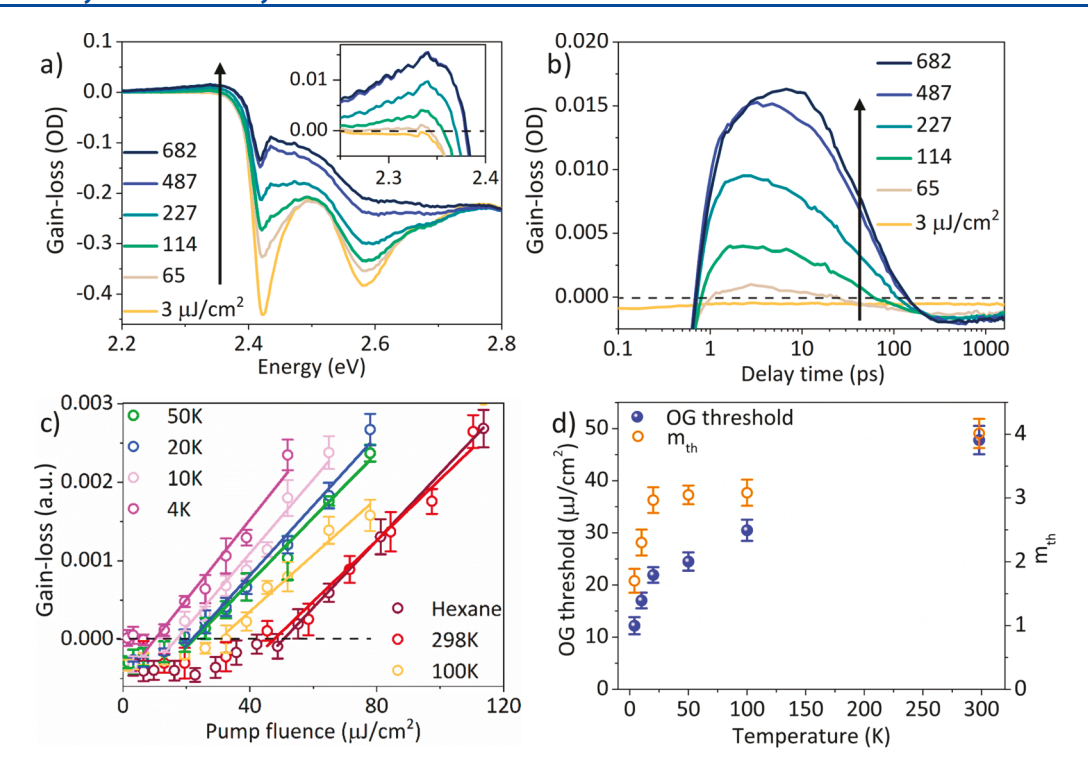


Figure 2. Temperature-dependent optical gain (OG) thresholds of CdSe NPLs. (a) Gain spectra, $-\Delta Abs(E, t) - Abs(E)$ (gain -loss), of NPL1 in hexane at 2–3 ps at indicated pump fluences with 3.1 eV excitation. The inset shows the same spectra in the OG region. (b) OG kinetics (probed at \sim 2.34 eV) of NPL1 in hexane at different pump fluences. (c) Normalized OG amplitude (at \sim 2.34 eV, 2–3 ps) at different temperatures as a function of pump fluence, where the intercept on the x-axis (black dashed line) gives the OG threshold. (d) OG threshold and average exciton number per NPL at the OG threshold (m_{th}) of NPL1 in hexane as a function of temperature.

Table 1. Exciton and Gain Parameters of NPL1 as a Function of Temperature

	hexane (298 K)	PMAO (298 K)	PMAO (100 K)	PMAO (50 K)	PMAO (20 K)	PMAO (10 K)	PMAO (4 K)
$I_{\rm th}~(\mu {\rm J/cm^2})$	50.7 ± 2.1	47.8 ± 2.7	30.5 ± 2.0	24.5 ± 1.2	21.9 ± 1.5	17.0 ± 1.5	12.2 ± 1.6
OD	0.34	0.24	0.29	0.18	0.12	0.15	0.19
$\varepsilon~(\times 10^5~{\rm cm}^{-1})$	1.17	1.17	1.48	1.62	1.66	1.71	1.85
$m_{ m th}$	3.83 ± 0.16	4.01 ± 0.23	3.08 ± 0.20	3.05 ± 0.15	2.97 ± 0.20	2.30 ± 0.20	1.70 ± 0.19
$S_{\rm X}~({\rm nm}^2)$	95.9 ± 15.4	95.3 ± 15.3	115.7 ± 15.6	123.4 ± 14.8	130.1 ± 13.9	137.5 ± 14.1	155.3 ± 12.5
$N_{ m S}$	3.50 ± 0.02	3.52 ± 0.02	2.90 ± 0.02	2.72 ± 0.02	2.58 ± 0.02	2.44 ± 0.02	2.16 ± 0.02

^aThese parameters include the temperature-dependent OG threshold ($I_{\rm th}$), optical density (OD) at 3.1 eV, NPL extinction coefficient per unit NPL volume (ε) at 3.1 eV, average exciton number per NPL at the OG threshold ($m_{\rm th}$), band-edge exciton coherent area ($S_{\rm X}$), and saturation number of band-edge excitons per NPL ($N_{\rm S}$).

normalized ultraviolet—visible absorption spectra of NPL1 at selected temperatures (Figure 1b) show two sharp peaks that can be attributed to the band-edge electron-heavy hole (A) and electron-light hole (B) exciton transitions (Figure 1c). The exciton peaks of NPL1 in PMAO drop compared to that in hexane at 298 K, which is likely due to the scattering from the NPL polymer film. Both A and B exciton peaks shift to higher energies at a lower temperature (from \sim 2.42 eV at 298 K to \sim 2.53 eV at 4 K) due to Varshni behavior. 31,32

The OG thresholds of NPL1 temperatures from 4 to 298 K were measured by pump fluence-dependent TA spectroscopy studies using 3.1 eV excitation. The optical density of the sample under illumination is $\Delta \text{Abs}(E,t) + \text{Abs}(E)$, where $\Delta \text{Abs}(E,t)$ is the photoinduced absorbance change measured in TA spectra and Abs(E) is the static absorbance before pump at energy E. Therefore, the OG threshold is reached when the gain is larger than the loss, i.e., $\Delta \text{Abs}(E,t) + \text{Abs}(E) < 0$. The gain spectra, expressed as $-[\Delta \text{Abs}(E,t) + \text{Abs}(E)]$, at 2–3 ps of NPL1 in hexane (298 K) at different pump fluences (Figure

2a) show a broad positive peak centered at ~2.34 eV, indicating the presence of OG in these samples. 18,33 The kinetics of NPL1 at OG peak energy (~2.34 eV) for different pump fluences are compared in Figure 2b. These kinetics show a negative signal around time zero (<~1 ps), which reflects a red-shifted exciton absorption caused by exciton-exciton interaction. 13,19,34 After ~ 1 ps, the OG amplitude remains negative at low pump fluences ($<3 \mu \text{J/cm}^2$), indicating gain <loss, while the OG amplitude becomes positive at a higher pump fluence (>65 μ J/cm²), indicating gain > loss. NPL1 in PMAO at different temperatures was also analyzed in the same way (Figure S5), and their OG peaks are at \sim 2.44, \sim 2.45, and \sim 2.46 eV at 100, 50, and 4–20 K, respectively. Note that at low temperatures ($\leq 100 \text{ K}$), an additional peak at $\sim 50 \text{ meV}$ higher than the OG peak appears at a high pump fluence $(>100 \,\mu\text{J/cm}^2)$, which is attributed to the OG from the excited state (p state) of the A exciton (Figure S5b-f).35

The OG amplitude reaches its maximum at a delay time of 2-3 ps (Figure 2b and Figure S5g-1), after which it decays

The Journal of Physical Chemistry Letters

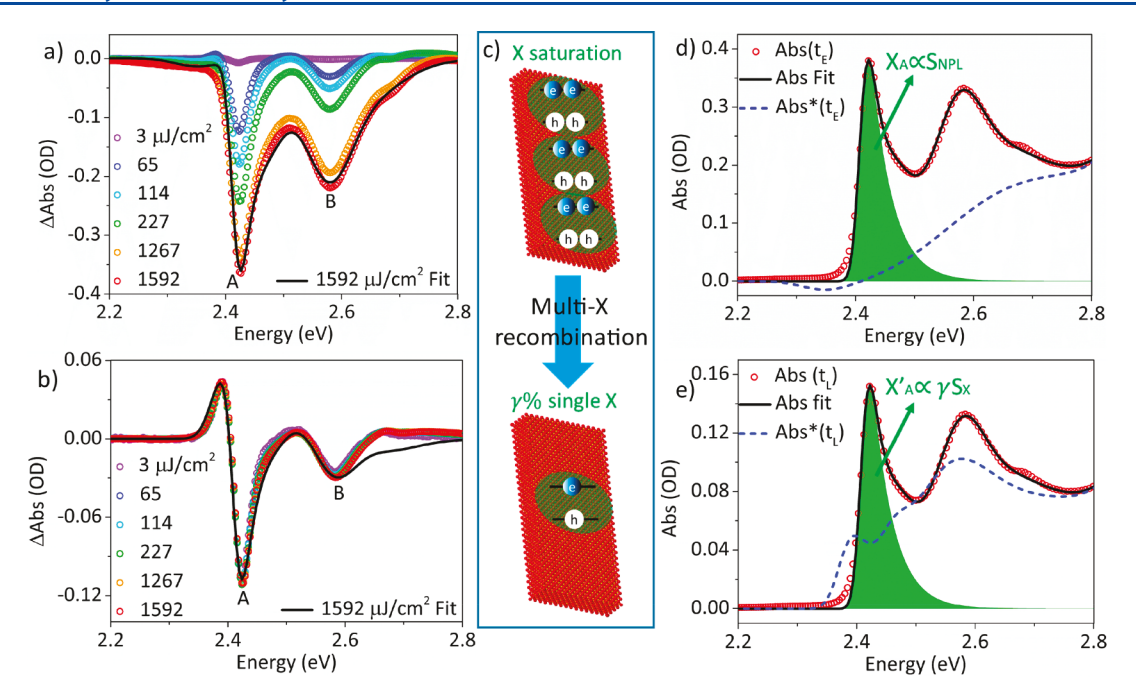


Figure 3. Pump fluence-dependent TA spectra of NPL1 in hexane at room temperature (298 K). (a) TA spectra at early delay times ($t_E = 2-3$ ps) and (b) normalized TA spectra at late delay times ($t_L = 800-1000$ ps) of NPL1 at indicated pump fluences (circles). Solid lines are the fits of TA spectra at the highest pump fluence (1592 μ J/cm²). (c) Schematic depiction of decay from the initial multiexciton state with a saturated number of band-edge excitons to the final single exciton state. The saturation number of the initial band-edge exciton is determined by the exciton spatial area (S_X) and the lateral size of NPLs (S_{NPL}) determined by TEM. Fits of the absorption spectra of the excited region in NPL1 NPLs before pump (Abs, solid black lines) and after pump (Abs*, blue dashed lines) at (d) early delay times ($t_E = 2-3$ ps) and (e) late delay times ($t_L = 800-1000$ ps) at the highest pump fluence (1592 μ J/cm²). Red circles show the normalized static absorption spectra of NPL1. Green shaded regions represent the A exciton absorbance in NPL1 NPLs before pump.

due to multiexciton annihilation. ^{13,18} A plot of the peak OG amplitudes as a function of pump fluence (Figure 2c) shows a linear dependence for gain > 0. We fit the peak OG amplitudes in their linear growth region for all temperatures (solid lines in Figure 2c) and extract the intercepts to determine the OG threshold fluence, which, as shown in Figure 2d, decreases from $47.8 \pm 2.7 \,\mu\text{J/cm}^2$ at 298 K to $12.2 \pm 1.6 \,\mu\text{J/cm}^2$ at 4 K (Table 1). The OG threshold at 298 K is consistent with previously reported values for CdSe NPLs, ^{33,36} even though a quantitative comparison of OG threshold values among different reports is difficult due to variations in optical densities, excitation wavelengths, and sample qualities.

The measured OG threshold fluence is related to the average exciton number per NPL at the OG threshold ($m_{\rm th}$) through eq 1.

$$I_{\rm th} = m_{\rm th} N_{\rm NPL} L \frac{hv}{1 - 10^{-\rm OD}} = m_{\rm th} \frac{hv}{\varepsilon V_{\rm NPL}} \frac{\rm OD}{1 - 10^{-\rm OD}}$$
 (1)

where $I_{\rm th}$ is the pump fluence (energy per unit excited area per pulse) at the OG threshold, $h\nu$ is the excitation photon energy (3.1 eV), $N_{\rm NPL}$ is the number of NPLs per unit volume, OD = $\varepsilon V_{\rm NPL} N_{\rm NPL} L$ (Beer's law) is the optical density at excitation energy, ε is the single NPL extinction coefficient per unit NPL volume, L is the sample thickness (1 mm in this work), and $V_{\rm NPL}$ is the volume of NPLs, which is calculated from its area [201.4 \pm 32.4 nm³ (Figure 1a)] and thickness (1.2 nm²6). ε (at 3.1 eV) is estimated to be 1.17 \times 10⁵ cm²1 at 298 K according to the reported extinction coefficient of the A exciton peak, 16 and its values at lower temperatures are estimated by both comparing the optical density of the same spot on the NPL1–PMAO film at different temperatures

(Figure S7b and Table 1) and comparing the results to those of absorption studies at reduced temperatures.³² From the measured threshold fluence and using eq 1, the average number of excitons at the gain threshold, $m_{\rm th}$, is determined to decrease from 4.01 ± 0.23 at 298 K (in PMAO) to 1.70 ± 0.19 at 4 K (Figure 2d and Table 1), indicating that four and more exciton states are required to reach the OG threshold at room temperature while the biexciton state is enough to achieve net OG at 4 K.

According to optical gain models of NPLs and QDs, ^{11,18} OG requires that the band-edge exciton states be at least half-filled, at which point the probability of stimulated emission equals the probability of absorption. As shown in Figure 2d, the average number of excitons per NPL at the OG threshold decreases with a decrease in temperature. This would suggest that the number of band-edge exciton states decreases at lower temperatures, which is possible if the exciton COM coherent spatial area increases at lower temperatures, as indicated in Scheme 1b.

To provide experimental support for the temperature-dependent exciton coherent spatial area $(S_{\rm X})$, we develop a new method for directly measuring its value in CdSe NPLs at different temperatures by pump fluence-dependent TA spectroscopy (at 3.1 eV excitation). This method is based on the determination of the number of band-edge excitons at saturation fluences. The comparison of TA spectra of NPL1 at early delay times $(t_{\rm E}=2-3~{\rm ps})$ measured with different pump fluences (Figure 3a) shows the bleach of A and B exciton bands, which can be attributed to the state filling of the lowest CB electron level,³⁴ similar to the case for cadmium chalcogenide QDs.^{37,38} This conclusion differs from those of some studies that report that the VB hole contributes to the

The Journal of Physical Chemistry Letters

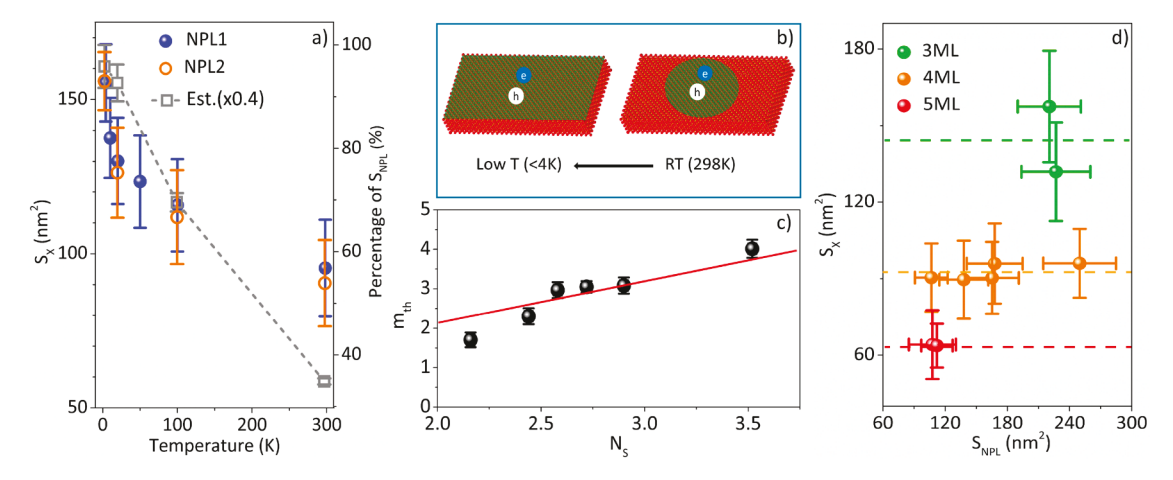


Figure 4. Temperature- and size-dependent S_X of CdSe NPLs. (a) Comparison of experimental S_X values of NPL1 (blue spheres) and NPL2 (orange circles) and estimated S_X values (Est., gray squares) as a function of temperature. The *y*-axis on the right represents the percentage of the lateral area of NPL1. (b) Scheme of S_X of CdSe NPLs at room temperature (RT, 298 K) and low temperature (low T_X <4 K). (c) Average exciton number per NPL at the gain threshold (m_{th}) as a function of the saturation number of band-edge excitons of NPLs (N_S). (d) N_S of CdSe NPLs with different thicknesses as a function of NPL lateral area. The dashed lines represent the average N_S for three-monolayer (green), four-monolayer (orange), and five-monolayer (red) CdSe NPLs.

exciton bleach signal. 39,40 The lack of hole state filling-induced exciton bleach signals has often been attributed to the higher degeneracy of VB levels, 37,38 which is also likely to be valid in NPLs due to the nonconfined lateral dimensions with a large effective mass of the heavy hole.⁶ With increasing pump fluences, both A and B exciton bleach amplitudes increase because there are more excited NPLs and more excitons per NPL. At pump fluences of >1267 μ J/cm², the A exciton bleach amplitude saturates, indicating the complete filling of the bandedge exciton states. Although the B exciton bleach should follow the same dependence on the pump fluence as the A exciton, its saturation behavior cannot be observed because this signal overlaps with a continuum feature associated with the A exciton band as shown in Supporting Information section S5. Furthermore, in addition to an exciton bleach, the presence of multiexcitons introduces other spectral features that give rise to the pump fluence-dependent TA spectral shape (Figure 3a).

The normalized TA spectra at late delay times (800-1000 ps) measured at different pump fluences are identical (Figure 3b), indicating that at this delay time, multiexciton states generated at high pump fluences have recombined, and only the single-exciton state remains. 13,15,41 This multiexciton decay process can be better seen in the A exciton bleach kinetics at different pump fluences (Figure S6a), which clearly shows an increase in the amplitude of the fast decay components at higher pump fluences, consistent with the expected increase in multiple-exciton populations. It also shows that both amplitudes at early delay times (2-3 ps) and late delay times (800-1000 ps) are saturated at high pump fluences when all NPLs in the probe beam path are excited, suggesting that all band-edge A exciton states are occupied at early delay times and these multiexciton states decay to a single-exciton state at late delay times (Figure 3c). Even at the lowest pump fluence $(3 \mu \text{J/cm}^2)$, with an estimated average exciton number per NPL of 0.04 (see Supporting Information section S4), the A exciton bleach decays to only $\gamma\%$ (68.9% in NPL1) of its initial amplitude at 1 ns. Note that this $\gamma\%$ factor accounts for both radiative and nonradiative decay of band-edge excitons. It may also contain relaxation between exciton fine structure states, particularly from bright to dark exciton state with a

reported splitting energy of \sim 5 meV for four-monolayer NPLs, 42 and exciton trapping with the electron in the CB edge and hole localized at a defect site within 1 ns. 43 The latter is expected to have a small or negligible effect on the exciton bleach amplitude.

The static absorption spectra of NPLs (black solid lines) can be well fitted to a model that consists of four absorption features: exciton bands along with continuous absorption bands of electron-heavy hole (A) and electron-light hole (B) transitions (Figure 3d,e). The absorption spectra after excitation (denoted as Abs*, blue dashed lines) can be fitted to a model that accounts for the state-filling-induced bleach of A and B exciton bands, the shift of A and B exciton frequency (due to exciton-exciton interaction), the bleach of the continuous absorption features, and band gap renormalizations (dashed lines in panels d and e of Figure 3).⁴⁴ Differences between these spectra (Abs* - Abs) yield the fit of the TA spectra at the saturation pump fluence (1592 $\mu \text{J/cm}^2$) shown in panels a and b of Figure 3 (solid lines). Details of the fitting procedures and results for all samples are shown in Supporting Information sections S5 and S6. According to the fit, at early delay times and saturation pump fluences (Figure 3d), when the A exciton is saturated, the A exciton bleach amplitude at $E_{\rm X}$ (peak of the A exciton transition) equals the A exciton absorbance of the whole NPL, $X_A(E_X)$, and is proportional to the area of the NPL (S_{NPL}) as shown in the top panel of Figure 3c. 16 At late delay times (Figure 3e), a single A exciton blocks half of the band-edge transitions within the exciton coherent area (due to 2-fold spin degeneracy in the CB level), leading to the bleach of half of the A exciton transitions in the same spatial area.44 The A exciton transitions outside the occupied area are unaffected so that they have no contributions to TA spectra at late delay times. Therefore, the A exciton absorbance of the excited region (i.e., the exciton coherent area) in an NPL at late delay times, $X_A'(E_X)$, which represents $\gamma\%$ of total NPLs with a single exciton, is proportional to $\gamma\% \times S_X$ (bottom panel of Figure 3c). This relationship is given by

$$\frac{X_{\rm A}(E_{\rm X})}{\frac{X_{\rm A}'(E_{\rm X})}{\gamma\%}} = \frac{S_{\rm NPL}}{S_{\rm X}} = \frac{N_{\rm S}}{2} \tag{2}$$

From the values of $X_A(E_X)/\{[X_A'(E_X)]/\gamma\%\}$ (1.75 \pm 0.01) and $S_{\rm NPL}$ [167.8 \pm 27.0 nm² (Figure 1a)], the value of S_X for NPL1 in hexane is determined to be 95.9 \pm 15.4 nm².

The TA spectra of NPL1 in PMAO at different temperatures were analyzed with the same method as described above, and all of the fitting results (Figure S11) and parameters (Table S5) are shown in Supporting Information section S6. S_x as a function of temperature is shown in Figure 4a, and their values are listed in Table 1. The result shows that S_X at a low temperature (4 K) occupies >90% of the NPL, extending nearly to the whole NPL area, as illustrated in Figure 4b. It also shows that the saturation number of band-edge excitons per NPL (N_S) is ~3.5 at room temperature and only ~2 at 4 K (Table 1). This is consistent with the change in $m_{\rm th}$ values determined by temperature-dependent OG threshold measurement (Figure 4c and Table 1), supporting the proposed gain model shown in panels a and b of Scheme 1. We observed similar temperature-dependent S_X of another four-monolayer CdSe NPL sample (NPL2) with a similar lateral area [165.3 \pm 25.8 nm² (Figure S1e)] in a different polymer, poly(methyl methacrylate) (PMMA), as shown in Figure 4a and Table S8.

Although changes in temperature can also affect the dielectric environment of the NPL, its effects on S_x can be excluded for two reasons. (1) The dielectric constant of nonpolar solids such as CdSe and PMAO changes negligibly with temperature. 45 (2) The measured $S_{\rm X}$ values do not show significant changes in solvents of different dielectric constants either (Figure S14 and Table S8). Exciton-phonon scattering, which decreases at low temperature due to a smaller phonon population, affects the exciton spatial coherence. The average spatial area resulted from this dephasing pathway can be estimated from the exciton line width according to the relationship $S_X = 4h^2/\Delta(T)M$, where h is Planck's constant, $\bar{\Delta}(T)$ is the transition line width at temperature T, and M is the sum of the effective masses of the band-edge electron (0.13 m_0 , where m_0 is the free electron mass) and hole $(0.89m_0)$. Using an emission line width of NPL2 at different temperatures of $\Delta(T)$ (Figure S15), the estimated S_X values calculated here (Figure 4a and Table S9) and in a previous study⁴¹ are >2-fold larger than our experimentally determined $S_{\rm x}$. This indicates that other factors besides exciton—phonon scattering play an essential role in reducing exciton spatial coherence. One reason is likely that the estimation is based on a perfect 2D quantum well with an infinite confinement potential and a constant density of states within the transition line width $[\Delta(T)]$, while the real NPLs have a thicknessdependent finite confinement potential, which changes the density of states and deviates from the perfect 2D quantum well. This is supported by the thickness-dependent S_X (Figure 4d): the thinnest three-monolayer NPLs possess an S_X (144.7 \pm 20.6 nm²) close to the estimated value (174 \pm 2 nm²) at room temperature. The thicker the NPLs, the larger the deviation from the estimated $S_{\rm x}$ despite the similar line width of three- to five-monolayer NPLs at room temperature (Figure S15b and Table S10). It has also been suggested previously that the inhomogeneity of the interaction between the surface capping ligand and NPL may play an important role.⁴⁶

We also studied how NPL thickness and lateral area affect S_X at room temperature using three-monolayer CdSe NPLs of two different sizes (3MLa and 3MLb), four-monolayer CdSe NPLs of three additional sizes (4MLa-c) besides NPL1 and NPL2, and five-monolayer NPLs of two different sizes (5MLa and 5MLb). These NPLs have increasing lateral sizes from a to c

(Figure S1), and their lateral sizes are determined in Table S1. The same set of samples has been used in studies of Auger recombination and optical gain of CdSe NPLs. 13,18 Using the same method, we extract the S_X values of these NPLs in hexane at room temperature (Table S1), which is independent of the lateral size but increases at smaller NPL thicknesses (Figure 4d). This indicates thinner NPLs may lead to lower OG thresholds. It is also important to note that our method for direct determination of exciton COM coherence applies to other semiconductor 2D and one-dimensional (1D) materials, which complements a previously reported method for estimation of the exciton Bohr radius in 1D nanotubes. 47,48

It is interesting to compare the temperature dependence of the gain threshold in materials of different dimensions. Nearly temperature-independent OG and ASE thresholds have been reported in zero-dimensional (0D) CdSe QDs¹ and 1D CdSe/ CdS NRs. 12 0D QDs are quantum-confined in all dimensions in which the exciton COM and the degeneracy of band-edge exciton states are temperature-independent; 1D cadmium chalcogenide NRs usually have non-uniform quantum confinement along their length direction, and this disorder reduces the exciton spatial coherence length dramatically. In conventional bulk semiconductor lasers, it has been reported that the gain threshold increases exponentially with temperature, which is due to the exponential absorption edge within the band gap induced by doping/defect states and the thermal spreading of carriers over a wide range of accessible electronic states near the band edge. 49,50 However, this does not apply to 2D NPLs, in which excitonic rather than free carrier transitions dominate at the band edge because of their large exciton binding energy (~100 meV). Unlike bulk semiconductors, the OG threshold of NPLs is determined by the relative populations of NPL species with different number of A excitons (Scheme 1).

We believe that our results provide not only a direct measurement of the exciton COM coherent area but also a new strategy for reducing the optical gain threshold in 2D NPLs. First, the exciton COM coherent delocalization is an important property in 2D materials as it determines the radiative recombination rate of band-edge excitons, the exciton transport mechanisms, and is the direct evidence of the GOST effect. Despite the importance, a reliable method for quantifying the exciton COM coherent area is lacking. Here we demonstrated a new method for directly quantifying the size of the exciton COM coherence for the first time. Moreover, for the first time, we clearly show that the exciton coherent area extends throughout the whole NPLs, providing the direct evidence of the GOST effect. Second, because of the ability to determine exciton COM directly, we discovered a new mechanism for efficiently reducing the OG threshold (by ~4-fold) of 2D NPLs by the GOST effect. It is important to emphasize that this exciton coherent area extension strategy reduces the OG threshold by achieving biexciton gain and enhancing the radiative recombination rate (GOST effect) without reducing the absorption cross section of 2D NPLs. We anticipate that this strategy for lowering gain thresholds is applicable in other 2D and 1D semiconductor nanomaterials that possess (1) uniform quantum confinement to enable large exciton spatial coherence and (2) a high exciton binding energy so that sharp excitonic transitions dominate at the band

In summary, we report a reduction of the OG threshold of 2D NPLs by exciton COM coherence extension and the GOST effect. The OG threshold of four-monolayer CdSe

NPLs decreases nearly 4-fold from \sim 48 μ J/cm² at room temperature to \sim 12 μ J/cm² at 4 K. TA spectroscopy studies show that the exciton COM coherent spatial area in CdSe NPLs is smaller than the NPL lateral size at room temperature and increases to nearly encompass the whole NPL at 4 K. Our result also shows that the exciton COM coherent spatial area at room temperature is independent of NPL lateral size but decreases in thicker NPLs. The reduction of the OG threshold at low temperatures is attributed to the extension of the exciton COM coherent area in NPLs, which reduces the saturation number of band-edge excitons to enable biexciton gain and increases the oscillator strength through the GOST effect. This work demonstrates a new approach for designing low-threshold optical gain materials.

METHODS

Synthesis of Three-Monolayer CdSe Colloidal NPLs. The CdSe colloidal NPLs were synthesized following the procedures reported in the literature with slight modifications. Typically, 170 mg of cadmium acetate dihydrate [Cd(Ac)₂·2H₂O] and 14 mL of 1-octadecene (ODE) were added to a 25 mL threeneck flask. After the mixture had been degassed under vacuum at 100 °C for 15 min, 12 mg of selenium powder in 1 mL of ODE was injected when the mixture was heated to 180 °C under an argon flow. The reaction continued for 5 and 10 min at 180 °C for 3MLa and 3MLb, respectively, and then was stopped with a water bath. One milliliter of oleic acid (OA) was injected into the solution at room temperature. The product was a mixture of CdSe NPLs and QDs, and the CdSe NPLs were separated from QDs by washing with an ethanol/ hexane mixture and centrifugation at 5000 rpm for 3 min. Final CdSe NPLs were dispersed in hexane.

Synthesis of Four-Monolayer CdSe Colloidal NPLs. First, 170 mg of cadmium myristate [Cd(myr)₂] and 14 mL of 1octadecene (ODE) were added to a 25 mL three-neck flask. After the mixture had been degassed under vacuum at 100 °C for 15 min, 12 mg of selenium powder in 1 mL of ODE was injected, and then the mixture was heated to 240 °C under an argon flow. When the temperature reached 200 °C, 40 mg of cadmium acetate dihydrate [Cd(Ac)2·2H2O] was introduced into the solution and heating continued. 4MLa was obtained by stopping the reaction when the temperature reached 230 °C. 4MLb, NPL1, NPL2, and 4MLc were obtained by reaction at 240 °C, and reactions continued for 1, 5, 5, and 15 min, respectively. Then the reactions stopped with a water bath. One milliliter of oleic acid (OA) was injected into the solution at room temperature. The products were a mixture of CdSe NPLs and QDs, and the CdSe NPLs were separated from QDs by washing with an ethanol/hexane mixture and centrifugation at 5000 rpm for 3 min. NPL2 was divided into three parts dispersed in hexane, toluene, and chloroform, while other samples were all dispersed in hexane.

Synthesis of Five-Monolayer CdSe Colloidal NPLs. First, 170 mg of cadmium myristate [Cd(myr)₂] and 14 mL of 1-octadecene (ODE) were introduced into a 25 mL three-neck flask. After the mixture had been degassed under vacuum at 100 °C for 15 min, the mixture was heated to 250 °C under an argon flow. When the temperature reached 250 °C, 12 mg of selenium powder in 1 mL of ODE was injected. After 60 s, 120 mg of cadmium acetate dihydrate [Cd(Ac)₂·2H₂O] was introduced into the solution. The reaction continued for 5 and 10 min at 250 °C for 5MLa and 5MLb, respectively, and then was stopped with a water bath. One milliliter of oleic acid

(OA) was injected into the solution at room temperature. The product was a mixture of CdSe NPLs and QDs, and the CdSe NPLs were separated from QDs by washing with an ethanol/hexane mixture and centrifugation at 5000 rpm for 3 min. Final CdSe NPLs were dispersed in hexane.

Sample Preparation for Low-Temperature Experiments. For NPL in polymer samples, the as-prepared colloidal NPLs were dried and redispersed in a saturated poly(maleic anhydride-alt-1-octadecene) (PMAO) or poly(methyl methacrylate) (PMMA) chloroform solution, placed on a sapphire substrate via the drop-casting method, and mounted in the cryostat. For NPL solid film samples, the as-prepared colloidal NPLs were dried and redispersed in a hexane/ethyl cyclohexane mixture. The redispersed NPLs were placed on a sapphire substrate via the drop-casting method and mounted in the cryostat.

Femtosecond Transient Absorption Setup. The femtosecond transient absorption measurements were taken in a Helios spectrometer (Ultrafast Systems LLC) with pump and probe beams derived from an amplified Ti:sapphire laser system (Coherent Legend, 800 nm, 150 fs, 2.4 mJ/pulse, 1 kHz repetition rate). The 800 nm output pulse was frequencydoubled to produce the 400 nm (3.1 eV) pump beam. A series of neutral-density filter wheels were used to adjust the power of the pump beam. The pump beam was focused on the sample with a beam waist of $\sim 300 \ \mu m$. A white light continuum (WLC) from 380 to 850 nm (from 1.5 to 3.3 eV) was generated by attenuating and focusing $\sim 10 \mu J$ of the 800 nm pulse on a rotating CaF₂ window. The WLC was split into a probe and reference beam. The probe beam was focused with an Al parabolic reflector onto the sample (with a beam waist of 150 μ m at the sample). The reference and probe beams were focused into a fiber-coupled multichannel spectrometer with complementary metal oxide semiconductor (CMOS) sensors and detected at a frequency of 1 kHz. The intensities of the pump and probe beams were tuned to correct for pulse-topulse fluctuation of the white light continuum. The delay between the pump and probe pulses was controlled by a motorized delay stage. The pump beam was chopped by a synchronized chopper to 500 Hz. The change in absorbance for the pumped and unpumped samples was calculated. Cuvettes (1 mm) were used for all solution sample spectroscopy measurements at room temperature. NPLs in PMAO or PMMA on the sapphire substrate were used for lowtemperature (<298 K) TA measurements. The instrument response function (IRF) of this system was determined to be \sim 150 fs by measuring solvent responses under the same experimental conditions (except a higher excitation power).

ASSOCIATED CONTENT

S Supporting Information

The Supporting Information is available free of charge on the ACS Publications website at DOI: 10.1021/acs.jp-clett.9b00759.

TEM images, additional transient absorption and photoluminescence spectra, kinetic fitting, and modeling details (PDF)

AUTHOR INFORMATION

Corresponding Author

*E-mail: tlian@emory.edu.

ORCID ®

Qiuyang Li: 0000-0002-8192-3960

Richard D. Schaller: 0000-0001-9696-8830 Tianquan Lian: 0000-0002-8351-3690

Notes

The authors declare no competing financial interest.

ACKNOWLEDGMENTS

This work was funded by grants from the National Science Foundation (CHE-1709182 and DMR-1629383). Use of the Center for Nanoscale Materials, an Office of Science user facility, was supported by the U.S. Department of Energy, Office of Science, Office of Basic Energy Sciences, under Contract DE-AC02-06CH11357.

REFERENCES

- (1) Klimov, V.; Mikhailovsky, A.; Xu, S.; Malko, A.; Hollingsworth, J.; Leatherdale, C.; Eisler, H. J.; Bawendi, M. Optical Gain and Stimulated Emission in Nanocrystal Quantum Dots. *Science* **2000**, 290, 314–317.
- (2) Asada, M.; Miyamoto, Y.; Suematsu, Y. Gain and the Threshold of Three-Dimensional Quantum-Box Lasers. *IEEE J. Quantum Electron.* **1986**, 22, 1915–1921.
- (3) Coleman, J. J.; Young, J. D.; Garg, A. Semiconductor Quantum Dot Lasers: A Tutorial. *J. Lightwave Technol.* **2011**, 29, 499–510.
- (4) Fan, F.; Voznyy, O.; Sabatini, R. P.; Bicanic, K. T.; Adachi, M. M.; McBride, J. R.; Reid, K. R.; Park, Y.-S.; Li, X.; Jain, A.; Quintero-Bermudez, R.; Saravanapavanantham, M.; Liu, M.; Korkusinski, M.; Hawrylak, P.; Klimov, V. I.; Rosenthal, S. J.; Hoogland, S.; Sargent, E. H. Continuous-Wave Lasing in Colloidal Quantum Dot Solids Enabled by Facet-Selective Epitaxy. *Nature* **2017**, *544*, 75–79.
- (5) Lim, J.; Park, Y.-S.; Klimov, V. I. Optical Gain in Colloidal Quantum Dots Achieved with Direct-Current Electrical Pumping. *Nat. Mater.* **2018**, *17*, 42–49.
- (6) Ithurria, S.; Tessier, M. D.; Mahler, B.; Lobo, R. P. S. M.; Dubertret, B.; Efros, A. Colloidal Nanoplatelets with Two-Dimensional Electronic Structure. *Nat. Mater.* **2011**, *10*, 936–941.
- (7) Grim, J. Q.; Christodoulou, S.; Di Stasio, F.; Krahne, R.; Cingolani, R.; Manna, L.; Moreels, I. Continuous-Wave Biexciton Lasing at Room Temperature Using Solution-Processed Quantum Wells. *Nat. Nanotechnol.* **2014**, *9*, 891–895.
- (8) She, C. X.; Fedin, I.; Dolzhnikov, D. S.; Demortiere, A.; Schaller, R. D.; Pelton, M.; Talapin, D. V. Low-Threshold Stimulated Emission Using Colloidal Quantum Wells. *Nano Lett.* **2014**, *14*, 2772–2777.
- (9) Yang, Z.; Pelton, M.; Fedin, I.; Talapin, D. V.; Waks, E. A Room Temperature Continuous-Wave Nanolaser Using Colloidal Quantum Wells. *Nat. Commun.* **2017**, *8*, 143.
- (10) Li, M.; Zhi, M.; Zhu, H.; Wu, W.-Y.; Xu, Q.-H.; Jhon, M. H.; Chan, Y. Ultralow-Threshold Multiphoton-Pumped Lasing from Colloidal Nanoplatelets in Solution. *Nat. Commun.* **2015**, *6*, 8513.
- (11) Klimov, V. I.; Ivanov, S. A.; Nanda, J.; Achermann, M.; Bezel, I.; McGuire, J. A.; Piryatinski, A. Single-exciton Optical Gain in Semiconductor Nanocrystals. *Nature* **2007**, *447*, 441–446.
- (12) Moreels, I.; Rainò, G.; Gomes, R.; Hens, Z.; Stöferle, T.; Mahrt, R. F. Nearly Temperature-Independent Threshold for Amplified Spontaneous Emission in Colloidal CdSe/CdS Quantum Dot-in-Rods. Adv. Mater. 2012, 24, OP231–OP235.
- (13) Li, Q.; Lian, T. Area- and Thickness-Dependent Biexciton Auger Recombination in Colloidal CdSe Nanoplatelets: Breaking the "Universal Volume Scaling Law. *Nano Lett.* **2017**, *17*, 3152–3158.
- (14) Pelton, M.; Andrews, J. J.; Fedin, I.; Talapin, D. V.; Leng, H.; O'Leary, S. K. Nonmonotonic Dependence of Auger Recombination Rate on Shell Thickness for CdSe/CdS Core/Shell Nanoplatelets. *Nano Lett.* **2017**, *17*, 6900–6906.
- (15) Kunneman, L. T.; Tessier, M. D.; Heuclin, H.; Dubertret, B.; Aulin, Y. V.; Grozema, F. C.; Schins, J. M.; Siebbeles, L. D. A. Bimolecular Auger Recombination of Electron-Hole Pairs in Two-Dimensional CdSe and CdSe/CdZnS Core/Shell Nanoplatelets. *J. Phys. Chem. Lett.* **2013**, *4*, 3574–3578.

- (16) Achtstein, A. W.; Antanovich, A.; Prudnikau, A.; Scott, R.; Woggon, U.; Artemyev, M. Linear Absorption in CdSe Nanoplates: Thickness and Lateral Size Dependency of the Intrinsic Absorption. *J. Phys. Chem. C* **2015**, *119*, 20156–20161.
- (17) Tessier, M. D.; Javaux, C.; Maksimovic, I.; Loriette, V.; Dubertret, B. Spectroscopy of Single CdSe Nanoplatelets. *ACS Nano* **2012**, *6*, 6751–6758.
- (18) Li, Q.; Lian, T. A Model for Optical Gain in Colloidal Nanoplatelets. *Chemical Science* **2018**, *9*, 728–734.
- (19) Li, Q.; Xu, Z.; McBride, J. R.; Lian, T. Low Threshold Multiexciton Optical Gain in Colloidal CdSe/CdTe Core/Crown Type-II Nanoplatelet Heterostructures. *ACS Nano* **2017**, *11*, 2545–2553.
- (20) Guzelturk, B.; Kelestemur, Y.; Olutas, M.; Li, Q.; Lian, T.; Demir, H. V. High-Efficiency Optical Gain in Type-II Semiconductor Nanocrystals of Alloyed Colloidal Quantum Wells. *J. Phys. Chem. Lett.* **2017**, *8*, 5317–5324.
- (21) Feldmann, J.; Peter, G.; Göbel, E. O.; Dawson, P.; Moore, K.; Foxon, C.; Elliott, R. J. Linewidth Dependence of Radiative Exciton Lifetimes in Quantum Wells. *Phys. Rev. Lett.* **1987**, *59*, 2337–2340.
- (22) Naeem, A.; Masia, F.; Christodoulou, S.; Moreels, I.; Borri, P.; Langbein, W. Giant Exciton Oscillator Strength and Radiatively Limited Dephasing in Two-Dimensional Platelets. *Phys. Rev. B: Condens. Matter Mater. Phys.* **2015**, *91*, 121302.
- (23) Griffin, G. B.; Ithurria, S.; Dolzhnikov, D. S.; Linkin, A.; Talapin, D. V.; Engel, G. S. Two-Dimensional Electronic Spectroscopy of CdSe Nanoparticles at Very Low Pulse Power. *J. Chem. Phys.* **2013**, *138*, 014705.
- (24) Caram, J. R.; Zheng, H.; Dahlberg, P. D.; Rolczynski, B. S.; Griffin, G. B.; Dolzhnikov, D. S.; Talapin, D. V.; Engel, G. S. Exploring Size and State Dynamics in CdSe Quantum Dots Using Two-Dimensional Electronic Spectroscopy. *J. Chem. Phys.* **2014**, *140*, 084701.
- (25) Cassette, E.; Pensack, R. D.; Mahler, B.; Scholes, G. D. Room-Temperature Exciton Coherence and Dephasing in Two-Dimensional Nanostructures. *Nat. Commun.* **2015**, *6*, 6086.
- (26) Biadala, L.; Liu, F.; Tessier, M. D.; Yakovlev, D. R.; Dubertret, B.; Bayer, M. Recombination Dynamics of Band Edge Excitons in Quasi-Two-Dimensional CdSe Nanoplatelets. *Nano Lett.* **2014**, *14*, 1134–1139.
- (27) Mahler, B.; Nadal, B.; Bouet, C.; Patriarche, G.; Dubertret, B. Core/Shell Colloidal Semiconductor Nanoplatelets. *J. Am. Chem. Soc.* **2012**, *134*, 18591–18598.
- (28) Gao, Y.; Weidman, M. C.; Tisdale, W. A. CdSe Nanoplatelet Films with Controlled Orientation of their Transition Dipole Moment. *Nano Lett.* **2017**, *17*, 3837–3843.
- (29) Rowland, C. E.; Fedin, I.; Zhang, H.; Gray, S. K.; Govorov, A. O.; Talapin, D. V.; Schaller, R. D. Picosecond Energy Transfer and Multiexciton Transfer Outpaces Auger Recombination in Binary CdSe Nanoplatelet Solids. *Nat. Mater.* 2015, 14, 484–489.
- (30) Guzelturk, B.; Erdem, O.; Olutas, M.; Kelestemur, Y.; Demir, H. V. Stacking in Colloidal Nanoplatelets: Tuning Excitonic Properties. ACS Nano 2014, 8, 12524–12533.
- (31) Varshni, Y. P. Temperature Dependence of the Energy Gap in Semiconductors. *Physica* **1967**, *34*, 149–154.
- (32) Diroll, B. T.; Fedin, I.; Darancet, P.; Talapin, D. V.; Schaller, R. D. Surface-Area-Dependent Electron Transfer Between Isoenergetic 2D Quantum Wells and a Molecular Acceptor. *J. Am. Chem. Soc.* **2016**, *138*, 11109–11112.
- (33) She, C.; Fedin, I.; Dolzhnikov, D. S.; Dahlberg, P. D.; Engel, G. S.; Schaller, R. D.; Talapin, D. V. Red, Yellow, Green, and Blue Amplified Spontaneous Emission and Lasing Using Colloidal CdSe Nanoplatelets. *ACS Nano* **2015**, *9*, 9475–9485.
- (34) Wu, K.; Li, Q.; Du, Y.; Chen, Z.; Lian, T. Ultrafast Exciton Quenching by Energy and Electron Transfer in Colloidal CdSe Nanosheet-Pt Heterostructures. *Chemical Science* **2015**, *6*, 1049–1054.
- (35) Achtstein, A. W.; Scott, R.; Kickhöfel, S.; Jagsch, S. T.; Christodoulou, S.; Bertrand, G. H. V.; Prudnikau, A. V.; Antanovich,

- A.; Artemyev, M.; Moreels, I.; Schliwa, A.; Woggon, U. p-State Luminescence in CdSe Nanoplatelets: Role of Lateral Confinement and a Longitudinal Optical Phonon Bottleneck. *Phys. Rev. Lett.* **2016**, *116*, 116802.
- (36) Olutas, M.; Guzelturk, B.; Kelestemur, Y.; Yeltik, A.; Delikanli, S.; Demir, H. V. Lateral Size-Dependent Spontaneous and Stimulated Emission Properties in Colloidal CdSe Nanoplatelets. *ACS Nano* **2015**, *9*, 5041–5050.
- (37) Klimov, V. I. Optical Nonlinearities and Ultrafast Carrier Dynamics in Semiconductor Nanocrystals. *J. Phys. Chem. B* **2000**, *104*, 6112–6123.
- (38) Hunsche, S.; Dekorsy, T.; Klimov, V.; Kurz, H. Ultrafast dynamics of carrier-induced absorption changes in highly-excited CdSe nanocrystals. *Appl. Phys. B: Lasers Opt.* **1996**, *62*, 3–10.
- (39) Cassette, E.; Pedetti, S.; Mahler, B.; Ithurria, S.; Dubertret, B.; Scholes, G. Ultrafast Exciton Dynamics in 2D In-Plane Hetero-Nanostructures: Delocalization and Charge Transfer. *Phys. Chem. Chem. Phys.* **2017**, *19*, 8373–8379.
- (40) Morgan, D. P.; Maddux, C. J. A.; Kelley, D. F. Transient Absorption Spectroscopy of CdSe Nanoplatelets. *J. Phys. Chem. C* **2018**, *122*, 23772–23779.
- (41) Ma, X.; Diroll, B. T.; Cho, W.; Fedin, I.; Schaller, R. D.; Talapin, D. V.; Gray, S. K.; Wiederrecht, G. P.; Gosztola, D. J. Size-Dependent Biexciton Quantum Yields and Carrier Dynamics of Quasi-Two-Dimensional Core/Shell Nanoplatelets. *ACS Nano* **2017**, *11*, 9119–9127.
- (42) Shornikova, E. V.; Biadala, L.; Yakovlev, D. R.; Sapega, V. F.; Kusrayev, Y. G.; Mitioglu, A. A.; Ballottin, M. V.; Christianen, P. C. M.; Belykh, V. V.; Kochiev, M. V.; Sibeldin, N. N.; Golovatenko, A. A.; Rodina, A. V.; Gippius, N. A.; Kuntzmann, A.; Jiang, Y.; Nasilowski, M.; Dubertret, B.; Bayer, M. Addressing the Exciton Fine Structure in Colloidal Nanocrystals: the Case of CdSe Nanoplatelets. *Nanoscale* 2018, 10, 646–656.
- (43) Kunneman, L. T.; Schins, J. M.; Pedetti, S.; Heuclin, H.; Grozema, F. C.; Houtepen, A. J.; Dubertret, B.; Siebbeles, L. D. A. Nature and Decay Pathways of Photoexcited States in CdSe and CdSe/CdS Nanoplatelets. *Nano Lett.* **2014**, *14*, 7039–7045.
- (44) Yang, Y.; Ostrowski, D. P.; France, R. M.; Zhu, K.; van de Lagemaat, J.; Luther, J. M.; Beard, M. C. Observation of a Hot-Phonon Bottleneck in Lead-Iodide Perovskites. *Nat. Photonics* **2016**, *10*, 53–59.
- (45) Young, K. F.; Frederikse, H. P. R. Compilation of the Static Dielectric Constant of Inorganic Solids. *J. Phys. Chem. Ref. Data* **1973**, 2, 313–410.
- (46) Rodina, A. V.; Golovatenko, A. A.; Shornikova, E. V.; Yakovlev, D. R.; Efros, A. L. Effect of Dangling Bond Spins on the Dark Exciton Recombination and Spin Polarization in CdSe Colloidal Nanostructures. *J. Electron. Mater.* **2018**, *47*, 4338–4344.
- (47) Mann, C.; Hertel, T. 13 nm Exciton Size in (6,5) Single-Wall Carbon Nanotubes. *J. Phys. Chem. Lett.* **2016**, *7*, 2276–2280.
- (48) Lüer, L.; Hoseinkhani, S.; Polli, D.; Crochet, J.; Hertel, T.; Lanzani, G. Size and Mobility of Excitons in (6, 5) Carbon Nanotubes. *Nat. Phys.* **2009**, *5*, 54–58.
- (49) Pankove, J. Temperature Dependence of Emission Efficiency and Lasing Threshold in Laser Diodes. *IEEE J. Quantum Electron.* **1968**, *4*, 119–122.
- (50) Ettenberg, M.; Nuese, C. J.; Kressel, H. The Temperature Dependence of Threshold Current for Double-Heterojunction Lasers. *J. Appl. Phys.* **1979**, *50*, 2949–2950.